A comparative study of force fields for predicting shape memory properties of liquid crystalline elastomers using molecular dynamic simulations

P. Prathumrat,[1] I. Sbarski,[1] E. Hajizadeh,[2] and M. Nikzad[1,a]

AFFILIATIONS

[1]Department of Mechanical and Product Design Engineering, Faculty of Science, Engineering and Technology, Swinburne University of Technology, John Street, Hawthorn, VIC 3122, Australia

[2]Department of Mechanical Engineering, Faculty of Engineering and Information Technology, University of Melbourne, Parkville, VIC 3010, Australia

[a]Author to whom correspondence should be addressed: mnikzad@swin.edu.au

ABSTRACT

Molecular dynamic (MD) simulation techniques are increasingly being adopted as efficient computational tools to design novel and exotic classes of materials for which traditional methods of synthesis and prototyping are either too costly, unsafe, and time-consuming in laboratory settings. Of such class of materials are liquid crystalline elastomers (LCEs) with favorable shape memory characteristics. These materials exhibit some distinct properties, including stimuli responsiveness to heat or UV and appropriate molecular structure for shape memory behaviors. In this work, the MD simulations were employed to compare and assess the leading force fields currently available for modeling the behavior of a typical LCE system. Three force fields, including Dreiding, PCFF, and SciPCFF, were separately assigned to model the LCE system, and their suitability was validated through experimental results. Among these selected force fields, the SciPCFF produced the best agreement with the experimentally measured thermal and viscoelastic properties compared to those of the simulated steady-state density, transition temperature, and viscoelastic characteristics. Next, shape fixity (R_f) and shape recovery (R_r) of LCEs were estimated using this force field. A four-step simulated shape memory procedure proceeded under a tensile mode. The changes in molecular conformations were calculated for R_f and R_r after the unloading step and reheating step. The results revealed that the model LCE system exhibit characteristic behaviors of Rf and Rr over the thermomechanical shape memory process, confirming the suitability of selected force field for use in the design and prediction of properties of typical LCE class of polymers.

I. INTRODUCTION

Shape memory elastomers (SMEs) are a significant member of intelligent polymers which can be deformed to another temporary shape and subsequently recovered to their permanent shape again.[1,2] This process is typically achieved through an applied load and forms of trigger by an external stimulus.[3] Currently, a variety of external stimuli are utilized to activate shape memory effects, including heat[4], pH[5], water[6], UV light[7], or electric and magnetic fields[8,9]. Among these, heat is the most commonly used stimulus. Furthermore, molecular architecture of these materials, containing net-points (hard phase) and switch units (soft phase), is the crucial determining factor which promotes the shape memory behavior.[10] The net-points responsible for maintaining the permanent shape are generated by covalent

1 or physical crosslinks.[11,12] Whereas, the switch units are responsible for maintaining the temporary shape as well as

2 recovering the permanent shape through transition temperature.[13] Therefore, these smart-functional SMEs can be

3 employed in a broad spectrum of applications such as medical devices[14,15], tissue engineering and soft robotics[16,17],

4 smart actuators[18], scaffold materials[19], and textiles[20].

5 Liquid crystalline elastomers (LCEs) serve as a distinct class of stimuli-responsive materials that contain the

6 ability to promote shape deformation by heat or UV activation.[21-23] These materials are a particular type of polymers

7 that contain the characteristics between solid crystalline materials and disordered liquids over a well-defined

8 temperature range.[24] The molecular structure of these materials consists of both hard and soft segments, enabling the

9 shape memory behaviors. Furthermore, transition temperature (T_{tran}) is an important parameter that plays a vital role

10 in the shape memory process. This parameter will serve as the switching point in the shape deformation step as well

11 as the recovery step. The LCEs naturally have several phase transitions, including the change from crystalline solid-

12 to-liquid-crystal (SLC) state followed by liquid-crystal-to-isotropic (LCI) state. Typically, majority of LCE materials

13 show at least two distinct transition phases, manifested through two transition temperatures (T_{tran}), including

14 crystalline-liquid crystal temperature (T_{SCL}) and liquid crystal-isotropic temperature (T_{LCI}). In the liquid crystal state,

15 the orientational order of LCEs can be classified as nematic, smectic, cholesteric, and discotic.[25] Among these, the

16 first synthesis of nematic LCEs has been reported by Finkelmann's method.[26]

17 In the last decade, LCEs have been developed for shape memory function based on variety of polymeric

18 systems, for instance, biphenyl-based epoxy[27], polyurethane LCEs (PULCEs)[28], as well as reactive mesogens

19 (RM).[29,30] Among these materials, RM has become an essential nematic LCE member to be utilized as SME due to

20 their ease of processability, excellent thermal, chemical, and mechanical stability.[31] For example, Traugutt et al.[30]

21 studied the effect of solvent presence on the shape memory characteristics of the LCEs based on 1,4-bis[4-(3-

22 acryloyloxypropypropyloxy) benzoyl-oxy]-2-methylbenzene (RM257), which were synthesized with 2,2′-

23 (ethylenedioxy)diethanethiol (EDDET) and pentaerythritol tetra (3-mercaptopropionate) (PETMP). The LCE

24 synthesized in the presence of the solvent possessed an R_f of 62.8% and R_r of 99.5%, greater than the case without the

25 solvent. Meanwhile, Barnes and Verduzco[32] studied the shape fixity and actuation as well as shape programming

26 behaviors of the RM257 synthesized through a two-step polymerization process in the presence of PETMP. These

27 studies highlight the LCEs based on RM257 as a promising class of polymers with further potential to develop and be

28 utilized for their shape memory functionalities, which can include applications such as artificial muscles for

29 bioengineering and controlled actuations of flaps and wings in aerospace engineering.[33,34]

30 With recent developments in materials simulation techniques and computational power, we now have a

31 powerful arsenal to tackle troubles associated with the common ad hoc trial-and-error experimental material

32 development approaches. Among these materials simulation methods, the molecular dynamic (MD) simulation

33 techniques offer a robust method that could potentially perform an essential role in predicting the macroscopic

34 behavior of materials from their microscopic structure, including their shape memory characteristics.[35,36] In the MD

35 simulation process, the force field, which defines the inter- and intramolecular interaction potentials in the materials

36 system, plays a central role in capturing the accurate time and length scales associated with molecular processes

1   determining the macroscopic behavior of the material.[35,37,38] Recently, this technique has been used to investigate

2   material properties and reproduce some experiments involving main-chain and side-chain LCEs.[39,40] Moreover,

3   several computational studies have been performed for the purpose of investigating the shape memory effects, where

4   depending on the polymeric system, different types of force fields have been employed. For instance, Diani and Gall[41]

5   implemented full-atomistic MD simulations using COMPASS (Condensed-phase Optimized Molecular Potential for

6   Atomistic Simulation Studies) force field to compare energy changes and strain recovery of natural rubber (cis-

7   polyisoprene) during the shape memory process. Their results revealed that this polymeric material can be fixed after

8   a uniaxial stretch below its T_g and recovered above its T_g. The conformational changes in this model polymer were

9   dictated by changes in entropy. Moon *et al.*[42] performed an all-atom MD simulation of polystyrene (PS) to investigate

10   the role of its initial orientational order on recovery behaviors, with the adoption of PCFF (Polymer Consistent Force

11   Field). This material indicated excellent R_f of 91.5% and R_r of 48.8% when sample was stretched up to 100% strain.

12   Such a high R_f of this material would be useful in the application of a controllable self-folding material. Yang *et al.*[43]

13   examined dynamic properties of epoxy networks with Diels-Alder reactions to understand shape memory behaviors

14   in atomistic scale by using the same PCFF potential. This thermosetting model demonstrated a high recovery rate at a

15   temperature of 350 K, which ranges from 0.00013 ps^{-1} to 0.00026 ps^{-1}, after stretched by 20%. Additionally, Zhang *et*

16   *al.*[44] also employed PCFF to explore the shape memory properties of amorphous poly(L-lactide) with different

17   molecular weights (M_w). The simulated R_r of PLLA decreased with an increase in M_w and remained in the range of

18   60%. Whereas, the R_f exhibited a value of up to 90%.

19   Nevertheless, very few studies address the suitability of the force field that could accurately capture the

20   structure and dynamics of these material systems. The most robust method to assess the suitability of a given force

21   field is to compare the simulation results of various force fields with the vital experimental characteristics of the same

22   material system. Lately, Wang *et al.*[45] have optimized the force fields of COMPASS and PCFF for a cellulose model.

23   In their work, steady-state density, the volatility, and repeatability of mechanical properties were the three essential

24   properties explored to compare the accuracy of these force fields. The results confirmed that the predicted properties

25   using COMPASS were in the best agreement with experimental data, resulting in the suitability for MD simulation of

26   this system. Moreover, Sahputra *et al.*[46] investigated the effects of tacticity, degree of polymerization, and temperature

27   on the elastic properties of poly(methyl methacrylate), (PMMA). The force fields, including Dreiding, AMBER

28   (Assisted Model Building with Energy Refinement), and OPLS (Optimized Potentials for Liquid Simulations), were

29   separately assigned to the model system. Their results indicated that the simulated Young's modulus and T_g by

30   Dreiding were in the closest fit with the experimental value when compared with other force fields. Therefore, to

31   achieve accurate and reliable simulated models of material, it is essential to critically evaluate the suitability of the

32   chosen force field for a particular material system.

33   In this study, given the rapidly evolving nature of the materials simulation techniques and underlying force

34   fields, it is critical that a suitable benchmark is established, and the optimal force field characteristics are identified.

35   Therefore, the MD simulations were utilized to compare the effectiveness of the choices of force fields and their

36   capability to accurately predict the shape memory characteristics of the LCEs through comparison by experimental

37   observations. The LCE based on 1,4-bis[4-(3-acryloyloxypropypropyloxy) benzoyl-oxy] -2-methylbenzene (RM257)

was first built in the simulation box and crosslinked with pentaerythritol tetra (3-mercaptopropionate) (PETMP) to form an elastomeric system. The force fields, including Dreiding, PCFF, and SciPCFF, were separately assigned to the simulated models. To conduct the experimental laboratory study, the LCE samples were synthesized to validate the accuracy of the predicted properties.[47] The material properties for evaluation and validation of the developed models were the steady-state density of the liquid crystalline monomers, the transition temperature of LCEs, and viscoelastic properties of LCEs. The force field, which showed the best agreement with the experimental data, was then adopted to investigate the shape memory characteristics, including R_f and R_r of the elastomeric system.

II. MATERIALS AND METHODS

A. Materials

The chemicals utilized in this study consisted of a reactive mesogen named 1,4-bis4-(3-acryloyloxypropypropyloxy) benzoyl-oxy] -2-methylbenzene (RM257), which was purchased from Daken Chemical (China). Pentaerythritol tetra (3-mercaptopropionate) (PETMP) based crosslinking agent and dipropyl amine (DPA) based catalyst were purchased from Sigma-Aldrich, Inc. (Australia). Toluene was purchased from Thermo Fisher Scientific Australia PTY LTD (Australia). All materials were used as received without further purification.

B. Synthesis of LCE

The synthesis procedure followed the method of Saed *et al.*[47] Briefly, powder of RM257 monomer was dissolved in 30 vol% of toluene and heated at 80ºC in an oven. The powder was dissolved entirely to be a transparent solution within 5 min. The solution was left to cool down to room temperature before proceeding to the next step. The 16 vol% of PETMP was then added and stirred to yield a homogenous mixture. DPA was separately diluted in toluene at a weight ratio of 1:50. Then, the 11 vol% of DPA was added into the monomer mixture, and all the constituents were instantaneously stirred. The solution was subsequently placed in a vacuum oven for 1 min for degassing to remove altogether. The mixture was immediately transferred into the mold and left at room temperature for 24 hrs to cure. After the polymerization was completed, the samples were heated at 80ºC for 12 hrs to remove the solvent before characterization.

C. Experimental

A differential scanning calorimeter (DSC) 2960 (TA instruments, USA) was used to characterize the thermal properties, including the transition temperatures of LCEs. The sample mass used was in the range of 5 mg to 10 mg sealed in an aluminum pan. The results were obtained using a heating rate of 5ºC/min with temperature ramped up from -40ºC to 150ºC under a nitrogen flow rate of 110 ml/min.

A dynamic mechanical analyzer (DMA) 2980 (TA instruments, USA) with tensile mode was utilized to measure the storage modulus and loss factor (tan delta) of the LCEs. The tests were run at 3ºC/min from room temperature to 150ºC. The frequency of 1 Hz and an amplitude of 15 μm were assigned for testing.

1   **D.   MD Simulation Protocol**

2   All MD simulations were performed by using the Materials and Process Simulation (MAPS) software

3 package (Version 4.3.0), developed by Scienomics Inc., France (2018). The simulations were run on the Ozstar High-

4 Performance Cluster (HPC) at the Swinburne University of Technology.

5   The chemical structures of RM257 monomer and PETMP crosslinking agent were built by using the sketching

6 tool on MAPS, as shown in Fig 1. The simulation box of the RM257 monomers was then created by using the

7 Amorphous Builder module. The force fields of Dreiding[48], PCFF[49], and SciPCFF (Scienomics Polymer Consistent

8 Force Field) were assigned to separate simulations. The parameters of SciPCFF have been developed by Scienomics

9 Inc. and extended from the PCFF version.[50,51] A set of equations of molecular interactions of these two force fields

10 are identical, including intramolecular, intermolecular, cross terms as well as quartic expansions of stretch and bend

11 in the potential energy calculations.[52] The SciPCFF, however, incorporates 9-6 Lennard-Jones (LJ) potentials and the

12 parameters of bond increment of various compounds from COMPASS.[53] The model was simulated using LAMMPS[54]

13 and relaxed via stepwise equilibration to conduct geometry minimization. The NVT and NPT ensembles of 1 ns at

14 298 K were then assigned to the system, respectively. The pressure of 1 atm was used in the NPT step. The steady-

15 state density of the liquid crystalline monomer was predicted with different force fields. The simulated density was

16 compared against the experimental density of RM257 monomer reported by the manufacturer, Daken Chemical.

17   The chemical structure of main-chain LCEs was also created using the sketching tool. The four-arm active

18 sites of PETMP (S-H bonds) were sketched to crosslink with the active sites (C=C bonds) at the ends of the RM257

19 structures. These LCE structures were then repeatedly sketched for 10 repeating units. Simulation box was finally then

20 constructed for the LCE structures using the Amorphous Builder module. Prior to calculation, the simulation box

21 included ten chains of the LCE structure were at a temperature of 298K. The final system had the empirical formula

22 of $C_{3810}H_{4040}O_{1240}S_{120}$ with the dimension of $46.642 \times 46.642 \times 46.642$ Å^3. The same simulation protocol, as explained

23 for the monomer model, was carried out for these materials. Briefly, the geometry of the LCE system was optimized

24 by using the steepest descent method for total running steps of 1000. The simulation box was then subjected to a 500

25 ps NVT step at 298 K. Nonbond interactions were conducted with a cutoff distance of 12 Å. A Nose-Hoover thermostat

26 was required to control the temperature with a damping coefficient of 10 fs. The Ewald summation was set to calculate

27 the Coulomb interactions. Subsequently, the NPT step was run with a dynamic time step of 1 ns. The same time step

28 was used at 298 K under a pressure of 1 atm. The Ewald summation method, and Nose-Hoover thermostat and barostat

29 was used with the same conditions as in the NVT step.

30   After reaching an equilibrium steady-state, transition temperature, and viscoelastic properties for different

31 models were calculated via the MAPS Trajectory Analysis module. The transition temperature was determined as the

32 point where the slope of the plot of fractional free volume (FFV) as a function of temperature changes. Meanwhile,

33 viscoelastic properties of the LCEs, including actual and relative storage moduli, and tan delta, were investigated from

34 components of the stress tensor using Trajectory Analysis module after the further NPT run of 10 ns with an amplitude

35 of 0.4 Å and period of shear of 5.0 ps.

1   **E.   Simulation of shape memory**

2   After the completion of force field comparison and selection, the simulated system with the best-agreed force

3   field, was subjected to the four-step procedure of shape memory process.[44]

4   First, in the loading step, the model was introduced into an NPT ensemble with a temperature of 400 K and

5   pressure of 1 atm. The uni-directional elongation was done in this step by stretching the simulation box with 10%

6   strain in the X direction, resulting in the deformation of the molecular chains. The duration of the run of 5 ns was used.

7   This is followed by a cooling step to freeze the stretched cell under an NVT ensemble for 500 ps at 298 K. Next, the

8   stored energy was released in the unloading step in an NPT ensemble. This step was set respectively under the

9   temperature and pressure of 298 K and 1 atm with a duration of 1 ns. Finally, the reheating step was run under the

10   NPT ensemble at 450 K with a pressure of 1 atm to relax the structure. A duration of 10 ns with a time step of 0.5 fs

11   was set in this step. The R_f and R_r were calculated using the strain data via Equations 1 and 2.

12
$$R_f = \frac{l_u}{l_m} \times 100\% \qquad (1)$$

13
$$R_r = \frac{l_m - l_p(N)}{l_m - l_p(N-1)} \times 100\% \qquad (2)$$

14   Where l_u is the fixed strain of the simulation box after stress relaxation, l_m is the maximum strain applied, l_p is the

15   residual strain after the recovery process, and N is the number of the cycles.

16

17   **III. RESULTS AND DISCUSSION**

18   **A.   Steady-state density analysis of the monomer model**

19   Fig. 1 illustrates the structural models of RM257 and PETMP monomers, constructed according to Section

20   II. The structure of the crosslinked main-chain LCEs were built through a two-step procedure, i.e., an initial sketch

21   were created using the sketching tool of MAPS and followed by using the amorphous builder module to build the LCE

22   model as shown in Fig 2. The LCE model was then assigned different force fields: Dreiding, PCFF, and SciPCFF. In

23   these simulations, some basic properties of the model materials can be calculated to assess the suitability of the force

24   field. The density of the simulated liquid crystalline monomer was probed to investigate and validate against the

25   experimental density value.

26   Fig. 3 shows the time-evolution of densities of RM257 monomer for different force fields. However, a

27   significant difference is observed for different force fields under ambient conditions. From the diagram, the density

28   from Dreiding, which is the generic or generic force field[55], exhibited a density of 1.073 g/cm^3. As we can see, this

29   applied force field reaches the steady-state slower than the others. It also exhibits a fluctuated behavior until the

30   equilibrium state is introduced after 500 ps of simulation. The density observed for this force field is inconsistent with

31   the reported density of 1.219 g/cm^3. This force field under-estimates the density by approximately 12%. In contrast,

32   the densities from the PCFF and SciPCFF, which developed as the second generation, rapidly reaches the equilibrium

state within 50 ps and 70 ps, respectively. The results were 1.158 g/cm^3 for PCFF and 1.202 g/cm^3 for SciPCFF. It can be seen that the overall trends of these two force fields are different from Dreiding. These behaviors could be a result of addition of the cross-terms and quartic terms for bonded and non-bonded interactions in these force fields. Compared with the experimental values, PCFF and SciPCFF under-predicted the density by approximately 5% and 2%, respectively. This difference in simulated density by these two force fields is explained by the coefficient variations used in defining the energy functions, indicating the possible best fit in SciPCFF terms used to predict the density of the polymeric systems[56].

The steady-state density data for the liquid crystalline monomer suggests that SciPCFF shows a more accurate prediction of the density of material than those obtained from the Dreiding, and PCFF. Based on this property, SciPCFF would be fit as an appropriate force field for the prediction of the properties of the LCE class of polymers. However, more validation with other material properties is necessary to further investigate its effectiveness.

B. Transition temperature of the elastomer model

The LCEs based on RM257 generally display nematic order in the liquid crystal phase. In this state, the molecules of LCEs have lost their positional order; however, the long-range orientational order still exists with their long axes, roughly parallel.[57] This behavior results in partial mobility of the molecules as a liquid while containing the orientational order as a crystalline solid. It is, therefore, called T_{tran} for this phase, which transfers the nematic liquid crystal to isotropic state, as nematic-isotropic temperature (T_{NI}). A measurement of the T_{tran} could be achieved using a variety of methods, including the free volume theory. An increment of the free volume of the material occurs as the temperature is increased. T_{tran} is defined as the temperature where an inflection in the specific volume-temperature curve emerges.

In this work, the fractional free volume (FFV) variation of LCE models as a function of temperature was studied as an efficient method for determining the T_{tran}. The ensemble-averaged free volume of the equilibrated LCE models in the NPT step were investigated by the Trajectory Analysis module. In our case, even though the LCEs contain two transition temperatures, including T_g and T_{NI}, we only focused on capturing the T_{NI} since this temperature is higher than ambient temperature. Meanwhile, the T_g of this material, which was measured by DSC, is -6ºC. Therefore, the utilization of the T_{NI} can prevent any interference from the surroundings, making it suitable to act as a switching temperature in the shape memory process. Fig. 4 illustrates the FFV of the elastomeric models with three force fields. The computational tests display a similar trend of volume expansion of the models with linear temperature changes. From the diagrams, it can be seen that the model demonstrates the linear response of the volume enhancement with increasing temperature. The increased slope of FFV exhibits weak first-order transition leading to dividing the slope into two lines. This transition behavior occurs due to small discontinuities in enthalpy, specific volume, and the fluctuation effect near the transition point.[58,59] The intersection of the slopes can be identified as T_{NI}. The predicted TNI by various force fields is included in Table I for comparison against the experimental results.

Fig. 5 shows the experimental T_{NI} investigated from tan delta data obtained from DMA test results, summarized in Table I. It is known that the transition temperatures obtained from DMA could be different from those

1 obtained from the free volume data analysis.[60] Additionally, the T_{NI} obtained from DSC is reported in this table. From

2 this figure, it can be mentioned that the maximum point of a tan delta curve represents the T_{NI}. This behavior agrees

3 with the results reported in Saed *et al*.[61] and Traugutt *et al*.[30] Table I shows that the T_{NI} values obtained from SciPCFF

4 are closest to the experimental results compared with those obtained using the other two force fields, with an under-

5 prediction of 12%. However, this discrepancy between simulation and experiment values may be affected by some

6 relevant factors such as the conversion degree of crosslinking reaction, or a heating rate. These parameters could vary

7 depending on the conditions of chemistry, stoichiometry or processing conditions.[62] Additionally, the T_{NI} value

8 predicted for the PCFF model is consistent with SciPCFF, yielding under-prediction by 17%. In contrast, Dreiding

9 over-predicts T_{NI} by 20%. These data show that SciPCFF results in more accurate values for this transition temperature

10 and shows a relatively good agreement with the experimental values. Consequently, it could confirm the accuracy of

11 this force field to be used for the simulation of LCEs.

12 Table I T_{NI} of LCE from simulations and experiments

	Dreiding	PCFF	SciPCFF	Experiment from DSC	Experiment from DMA (tan delta)
T_{NI} (ºC)	106	73	77	88	87

13

14 **C. Viscoelastic properties of the LCE model**

15 Storage modulus (E') and tan delta were the key viscoelastic properties investigated using MD simulations in

16 this study, which could potentially verify the suitability of the adopted force fields. These two properties were

17 experimentally evaluated in tensile mode and are shown in Fig. 5 as a function of temperature. The E' value at the

18 temperature of 27ºC is approximately 7.3 MPa. Moreover, to compare with the simulation results, the experimental E'

19 values at various temperatures of 47ºC, 67ºC and 87ºC are obtained from this figure and compared with the

20 corresponding values obtained from the MD simulations of different force fields in Fig. 6.

21 Fig.6 reveals that the E' data obtained for the SciPCFF model is the only force field that agrees well with the

22 experimental data for the entire temperature range. The E' data for this model shows a decreasing trend with increasing

23 temperature and exhibits values lower than the experimental results. In contrast, the E' data obtained from the PCFF

24 model shows a linear trend within the whole range of studied temperatures. Similar results are acquired from the

25 Dreiding model. This observation lies in the differences between these force fields as mentioned earlier. In particular,

26 the complexity of the force field, for example, Dreiding based generic force field and PCFF/SciPCFF based second

27 generation, has an essential effect on the accuracy of the predicted results. Moreover, differences in the coefficients

28 of the force fields and the functional form of various terms in the force fields result in the consistency of the

29 predictions.[63] Having compared all these three force fields, it is clear that only the SciPCFF potential is in good

30 agreement with the experiment. Nevertheless, the discrepancy between the E' values at low temperature compared

1   with the experimental data is still considerable. This inconsistency may occur due to the difference in the numbers of

2   atoms in the simulation box and the actual samples. Thus, further investigation is required; for example, an adaptation

3   of the cutoff distance and long-range interaction terms could reduce the discrepancy of this property. In addition, a

4   relative E' which compared to the reference E' was employed as well as the percentage average absolute relative errors

5   (AARE).[50]

6   The relative change in modulus E'/E'_r is further analyzed to determine the force field accuracy, where E'_r is

7   the reference modulus at 27°C and is illustrated in Fig. 7. E'/E'_r data reveals that SciPCFF is the only force field with

8   good agreement with the experimental results. Furthermore, %AARE was also computed, as presented in Table 2. The

9   %AARE measured in this paper are denoted as β_E and β_t and refer to the %AARE of modulus values and tanδ values,

10 respectively. β_E and β_t calculated using Equation 3 and Equation 4. The E'_s and tanδ_s are the predicted storage modulus

11 and tan delta by the model, respectively. The E'_{exp} and tanδ_{exp} are the experimental storage modulus and tan delta value

12 from DMA, respectively. N is the number of compositions with different temperatures (in this case, N = 4).

13
$$\beta_E = \frac{100}{N}\sum_{i=1}^{N}\left|\frac{E'_s - E'_{exp}}{E'_{exp}}\right| \tag{3}$$

14
$$\beta_t = \frac{100}{N}\sum_{i=1}^{N}\left|\frac{tan\delta_s - tan\delta_{exp}}{tan\delta_{exp}}\right| \tag{4}$$

15 Table II shows that SciPCFF results in the lowest β_E value of 52% among the three force fields, however, it is a

16 relatively high value compared to the experimental sample. This error analysis indicated that further improvements of

17 the simulated models or parameters of the force fields are required to achieve a greater consistency for the results. In

18 order to ensure that SciPCFF is the appropriate force field for this system, another viscoelastic property such as tan

19 delta was considered further.

20 Tan delta curve of the simulated LCE system is represented in Fig. 8. This property is the ratio of the

21 dissipated energy to the stored energy in various sample deformation processes.[64] In this figure, it can be seen that the

22 SciPCFF model shows a remarkable agreement with the experimental data. The trend of these two curves is consistent

23 with each other, along with the observed temperatures. In contrast, the trend of simulated tan delta for Dreiding and

24 PCFF potentials discrepant and are less concentrated when compared with the experiment work. The β_t of the

25 simulated tan delta is also reported in Table II. It can also be calculated by using Equation 4. The result confirms the

26 accuracy of SciPCFF, providing the value of 13%, following the experimental data value. This parameter can assist

27 in approaching accurate predictions of the viscoelastic properties. In comparison, SciPCFF again demonstrates an

28 excellent agreement with the experimental data.

29

30

31

1   Table II β_E and β_t value from storage modulus and tan delta obtained for different force fields when compared with

2   the experimental values

Force field	β_E of storage modulus	β_t of tan delta
Dreiding	170	24
PCFF	83	27
SciPCFF	52	13

3

4   Therefore, it is clear that the simulation results with SciPCFF exhibit the best agreement with the

5   experimental data. Particularly, these results emphasize the significance of addition of cross-terms and cubic expansion

6   of intramolecular bonds in the second-generation force fields to better enhance the accuracy of simulated model

7   systems in terms of potential energies, molecular conformation, and vibrational frequency.[52] In particular, the cross-

8   terms increase the transferability of the diagonal terms, including bond stretching, bond bending, torsion, and improper

9   torsion.[52] However, the Dreiding as a generic force field, only contains the computation of the squared degree of

10   intramolecular interactions without containing the series of cross-terms. Moreover, PCFF and SciPCFF employ 9-6

11   LJ potential to calculate van der Waals interactions between simple atoms and molecules[53,65], while, Dreiding uses

12   12-6 LJ potential[66], as shown in Equations 4 and 5. The attractive part of LJ potential, at long-range interactions or

13   dispersion force, is indicated by $(1/r)^6$.[67] Meanwhile, the repulsive part of LJ potential, describing the repulsion at short

14   distances of the interacting particles, can be varied by $(1/r)^{12}$ and $(1/r)^9$ depending on the types of force field. The

15   difference of exponent in the repulsive part of these equations has an essential impact on the accuracy of the predicted

16   properties. In this case, the high steep repulsive term of 12-6 LJ potential could affect an overestimation of the pressure

17   in the model.[67] This parameter, $(1/r)^{12}$, could lead to the rigor of attractive force between molecules. Therefore, a

18   replacement by $(1/r)^9$ represents a weaker repulsive part[67], allowing the molecules to move closer. At the same time,

19   an improvement of the second-generation force field, especially torsional potential, could necessarily affect the

20   structural conformation and bonding of liquid crystal materials, adapting the balance of repulsion and conjugation of

21   the polymeric system.[68] Based on these reasons, the PCFF and SciPCFF can have efficacy on modeling and validation

22   of the simulated LCE system and demonstrate more accurate results than Dreiding.

23
$$U_{LJ} = 4\varepsilon \left[\left(\frac{\sigma}{r} \right)^9 - \left(\frac{\sigma}{r} \right)^6 \right] \qquad (4)$$

24
$$U_{LJ} = 4\varepsilon \left[\left(\frac{\sigma}{r} \right)^{12} - \left(\frac{\sigma}{r} \right)^6 \right] \qquad (5)$$

25   Where ε is defined as the depth of the potential well, σ stands for distance at which the particle-particle potential

26   energy, and r is the distance between two interacting particles.

27   Furthermore, when comparing the effectiveness between PCFF and SciPCFF, which belong to the same force

28   field generation, these two force fields have the same energy functions for computing all inter- and intramolecular

1 interactions, as well as the cross-terms. However, the coefficients in some functions of SciPCFF are different from the

2 PCFF version, for instance, in quartic bonds and angles, torsion angles, improper angles, and cross-terms. It can be

3 clarified that the different coefficients in force field calculation can play a significant role in the development of

4 accuracy. Thus, the improved version of SciPCFF is the force-field of choice for studying shape memory

5 characteristics of this polymeric system.

6 **D. Prediction of shape memory properties of LCE**

7 After validations, SciPCFF is further utilized for the study of the shape memory properties of LCE. Fig. 9

8 displays a four-step thermomechanical protocol for the simulation of the shape memory process. A relevant loading

9 is applied to the simulation box during a loading step. The temperature is kept constant, and the simulation box is

10 strained with constant stress. Second, the temperature of the system is reduced to room temperature. While the assigned

11 load is still held in the system. In this step, it is clear that the conformation of the model is the same as the previous

12 steps. Third, the temperature is kept the same as the cooling step while the load is removed. The low temperature can

13 prevent the mobility of the polymeric chains and entropy-driven shape recoveries [42]. Eventually, the high temperature

14 at 450K is used to recover the sample to its original shape.

15 Changes in the chain conformation are calculated using Equations 1 and 2, respectively, through the R_f and

16 R_r. After the unloading step, the model exhibited an excellent R_f of about 97.9% $\pm$ 0.1%. This result reveals that the

17 model can be deformed and maintained well under the strain-controlled conditions. However, a small shrinkage

18 occurred rapidly after stress relaxation due to the total energy in the system.[69] This effect resulted in the unreachable

19 100% of R_f. However, the R_f values lie in the same range as reported in Saed *et al.*[47] and Martinez-Gomez *et al.*[70] In

20 addition, the R_r is computed to be approximately 73.8% $\pm$ 0.3%. This result is similar to the reported results of 80.3%

21 by Moon *et al.*[42] The unrecoverable strain from the heating step could be the result of disentanglement of the physical

22 entanglement of the polymeric chains during the mechanical deformation.[42,71]

23 Fig. 10 demonstrates the pressure applied in the simulation box for the various steps of the shape memory

24 process. The pressure is initially assigned to enforce the simulated sample to temporary shape deformation. When the

25 sample is cooled down with the constant volume, the pressure dramatically reduces due to a decrement of temperature.

26 The model also slightly recovered under the pressure of 1 atm at room temperature in an unloading step. However,

27 the stretched model maintained its temporary shape in the stretched direction (x dimension) due to the enforced

28 pressure during the cooling. This may also be caused by the lower mobility of the molecular chains in the simulation

29 box at room temperature. Finally, the stored dimension of this material partially disappeared when the temperature is

30 increased to 450 K under the same pressure of 1 atm.

31 The total energy changes during the thermomechanical shape memory process are shown in Fig. 11. The

32 model shows a 73% higher energy (9500 kcal/mol) compared to the following cooling step (2600 kcal/mol). The

33 residual energy stored in this cooling stage could affect conformational changes in this system. Even though the sample

34 is cooled down to room temperature, the molecular chain still shows some mobility possibly owing to this residual

35 energy. Therefore, achieving 100% fixity for this simulated model is not possible. This amount of energy also remains

1 at this level when the stress is removed in an unloading step. Eventually, the total energy rises to a high level at about

2 11200 kcal/mol when the temperature is increased up to 450 K for shape recovery. It can be seen that the total energy

3 of the various stages converges toward an equilibrium state. From these results, SciPCFF proves to be the best force

4 field to predict the shape memory characteristics of LCE-based RM257, and other intensive physiochemical and

5 mechanical properties.

6

7 **IV. CONCLUSION**

8   This research work represents a study on the assessment of appropriate force fields to capture the shape

9 memory properties of LCEs. The critical properties of this material, including steady-state density, transition

10 temperature, and viscoelastic properties, are characterized using both laboratory experiments and MD simulations.

11 The MD simulations of this elastomer are performed by assigning three different types of force fields, namely

12 Dreiding, PCFF, and SciPCFF. By comparing experimentally measured data with those obtained through MD

13 simulations, the accuracy of three force fields is discussed. The results show that the thermomechanical properties of

14 the system modeled by the SciPCFF potential agree well with the corresponding experimental data and are the most

15 accurate representation of the molecular interactions prevalent for the selected liquid crystalline elastomer. This force

16 field is then utilized to predict the shape memory properties of this system, including R_f and R_r, which are 97.9% $\pm$

17 0.1% and 73.8% $\pm$ 0.3%, respectively. Moreover, the total energy of each shape memory step reaches equilibrium

18 throughout the process, confirming that SciPCFF is the most appropriate force field to study the LCEs.

19

20 **ACKNOWLEDGEMENT**

24

25 **DATA AVAILABILITY**

26   The data that support the findings of this study are available from the corresponding author upon reasonable

27 request.

28

ACCEPTED MANUSCRIPT

Journal of
Applied Physics

This is the author's peer reviewed, accepted manuscript. However, the online version of record will be different from this version once it has been copyedited and typeset.
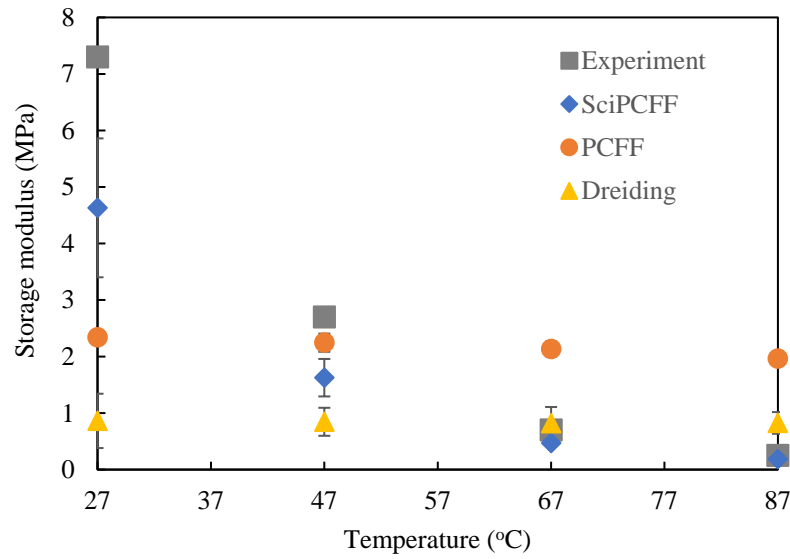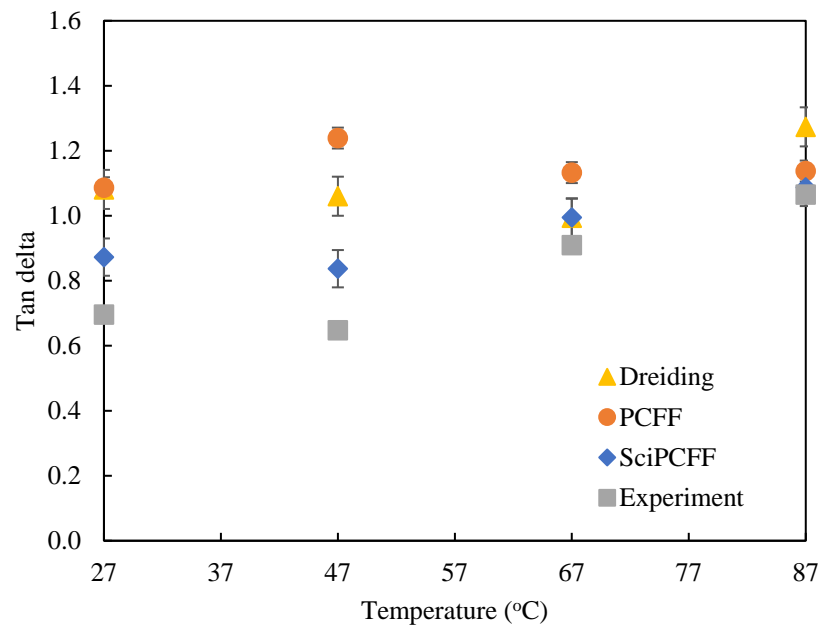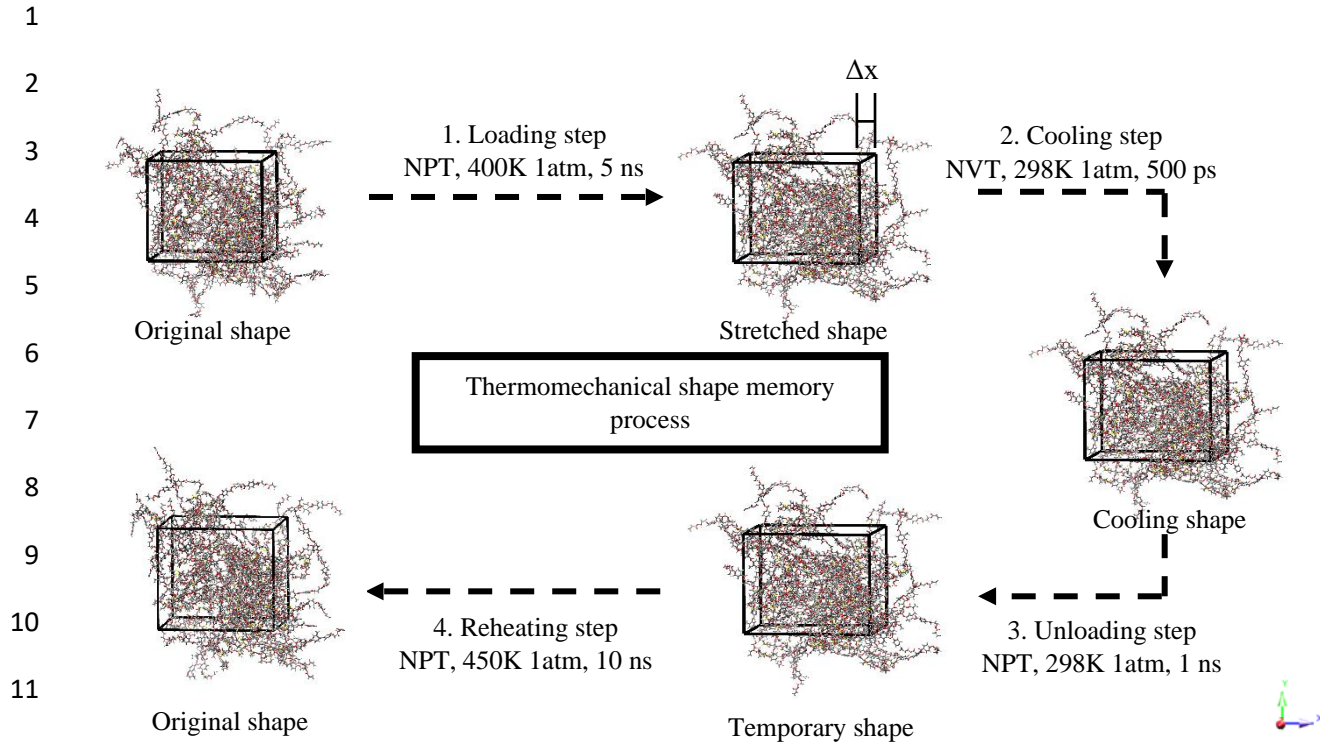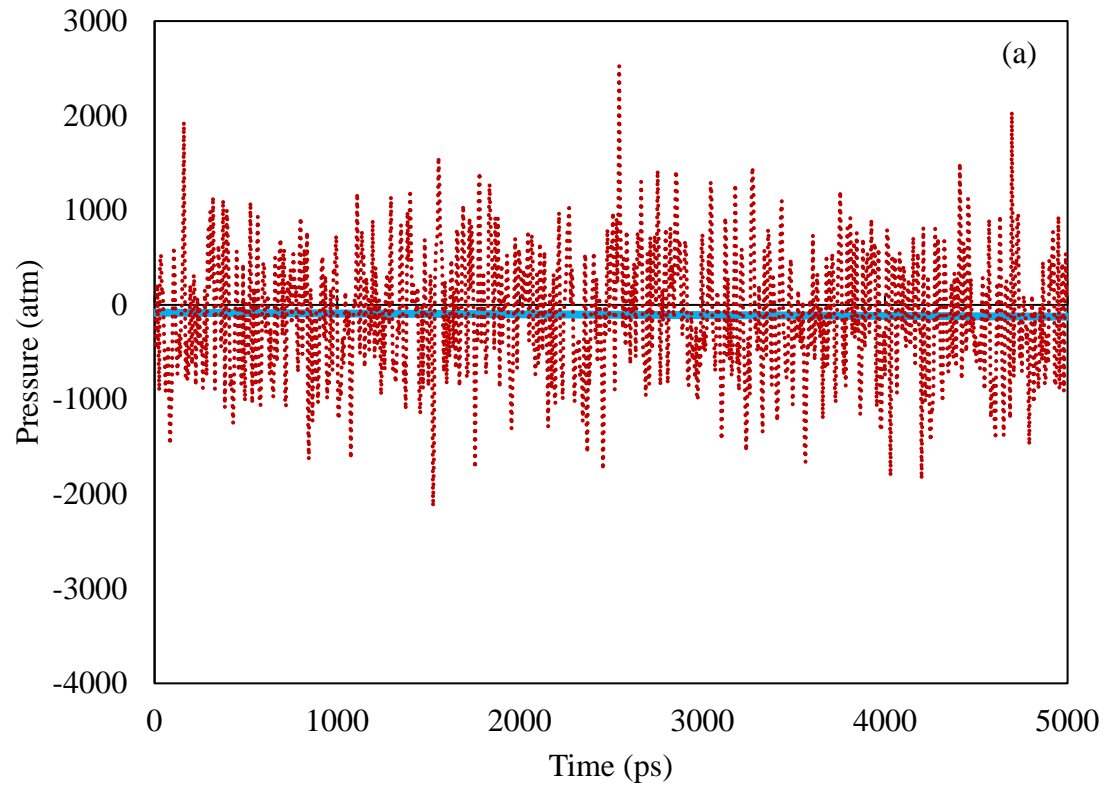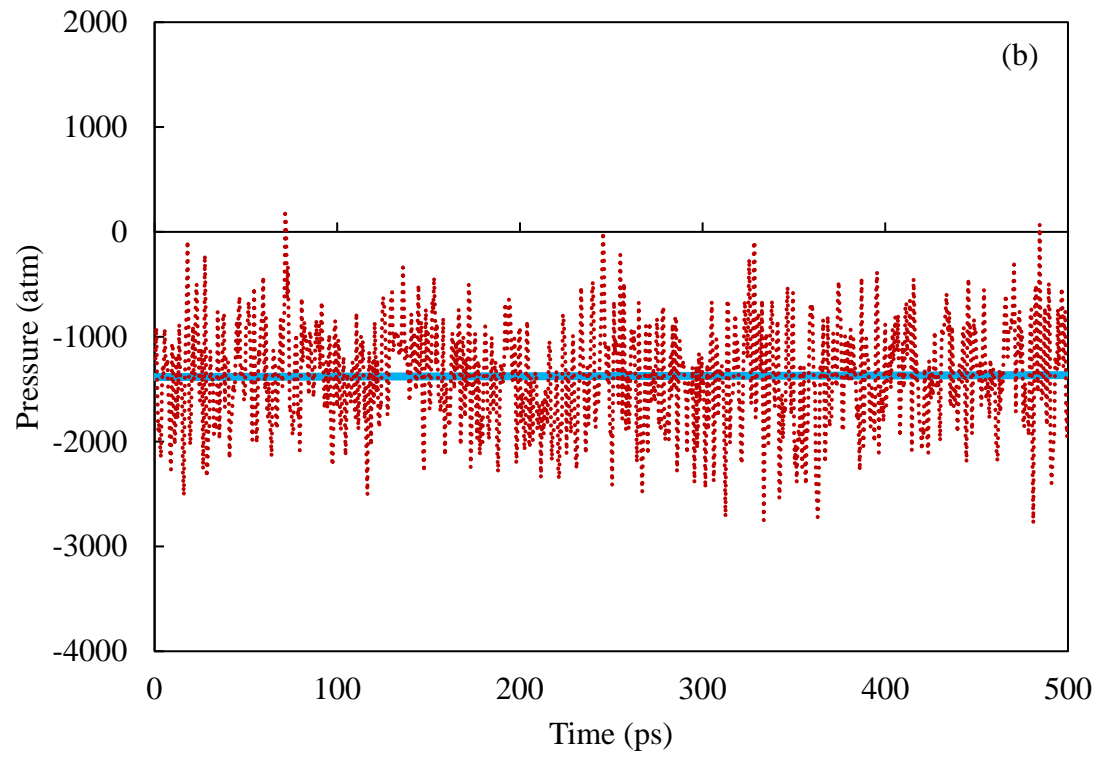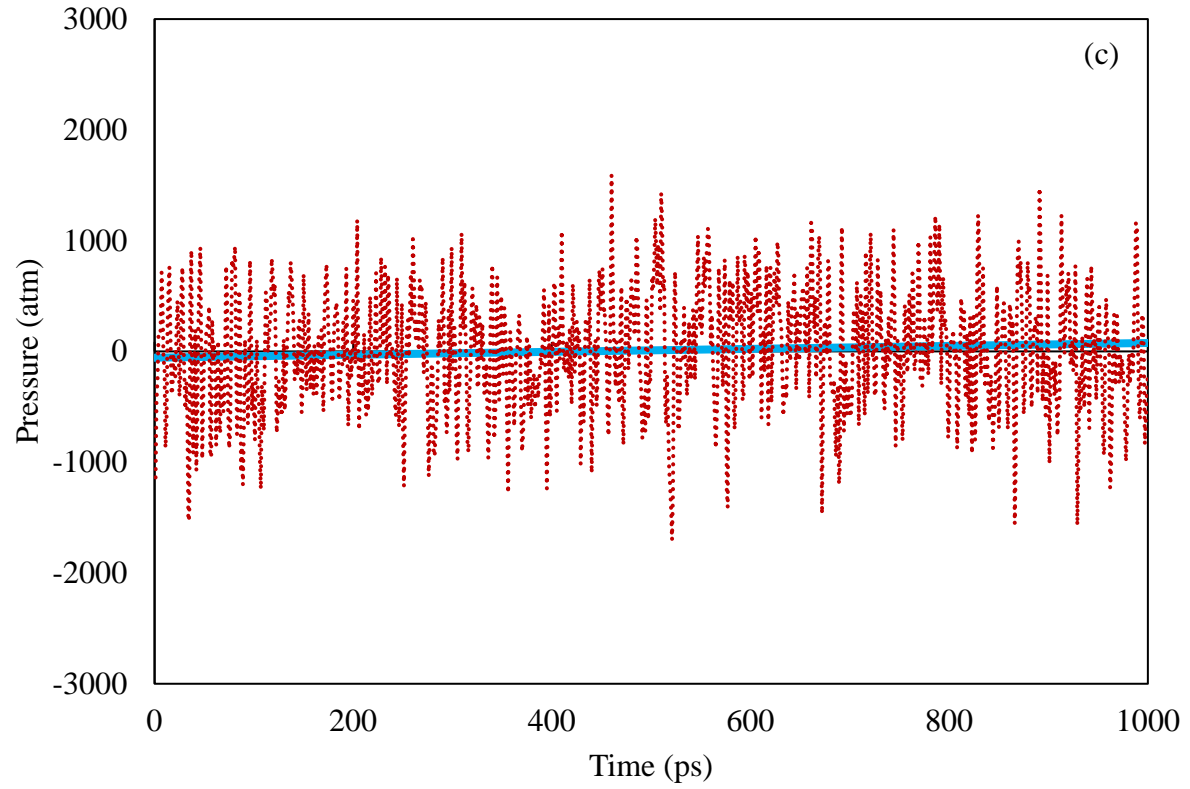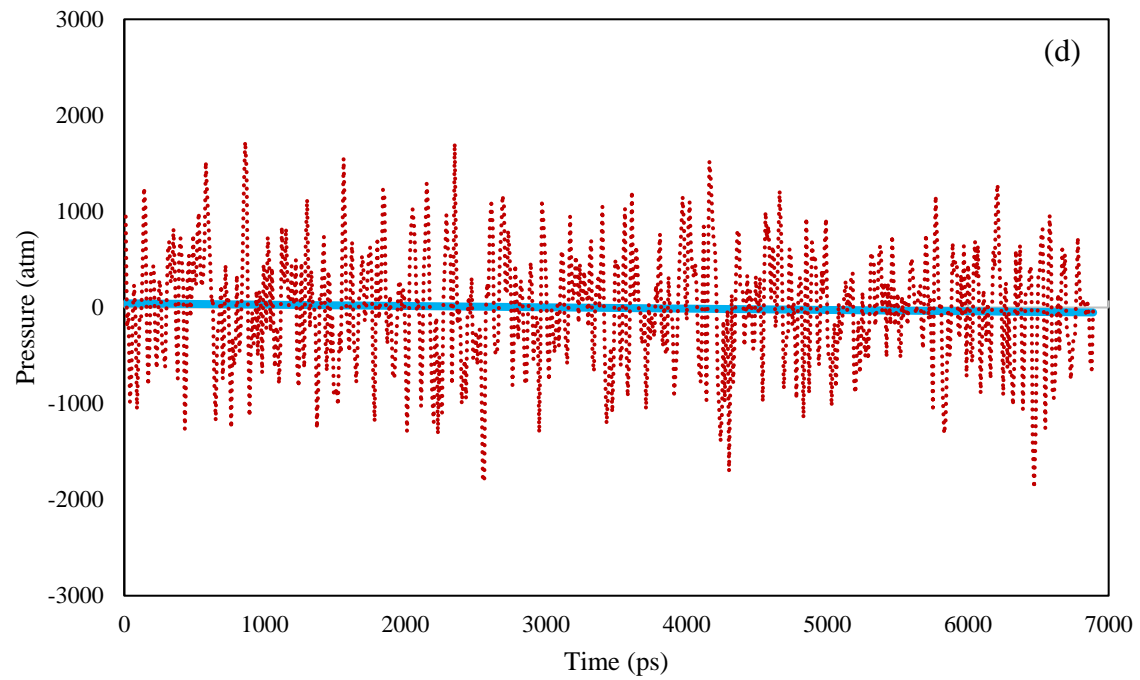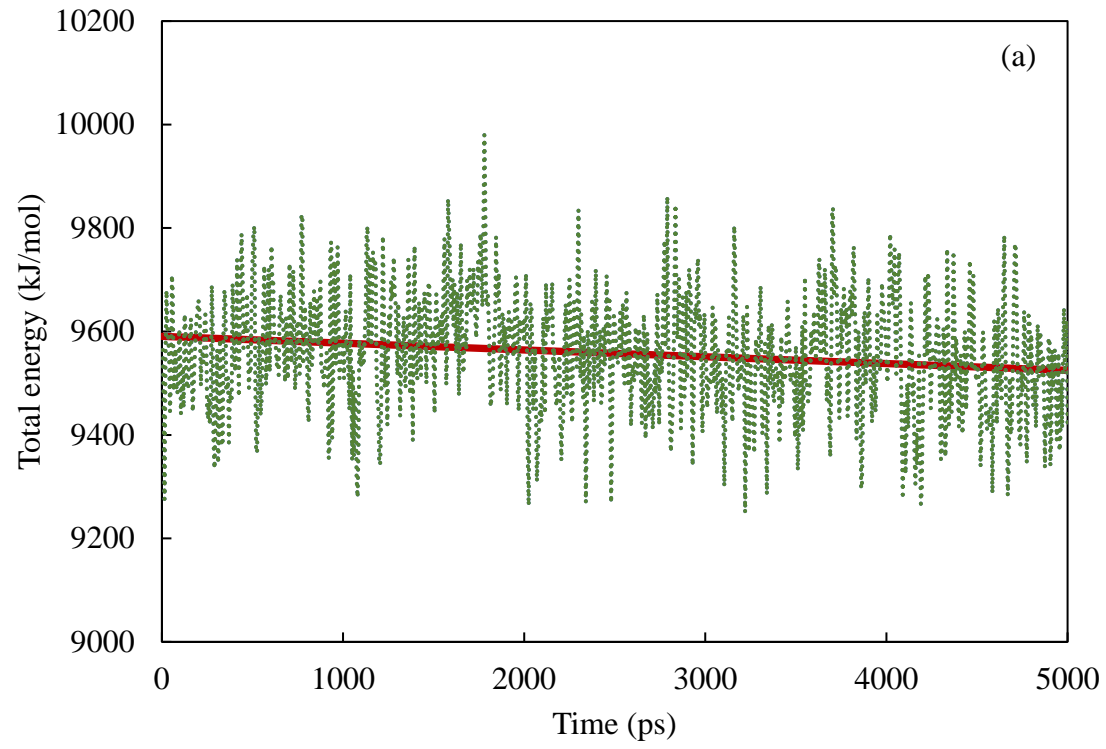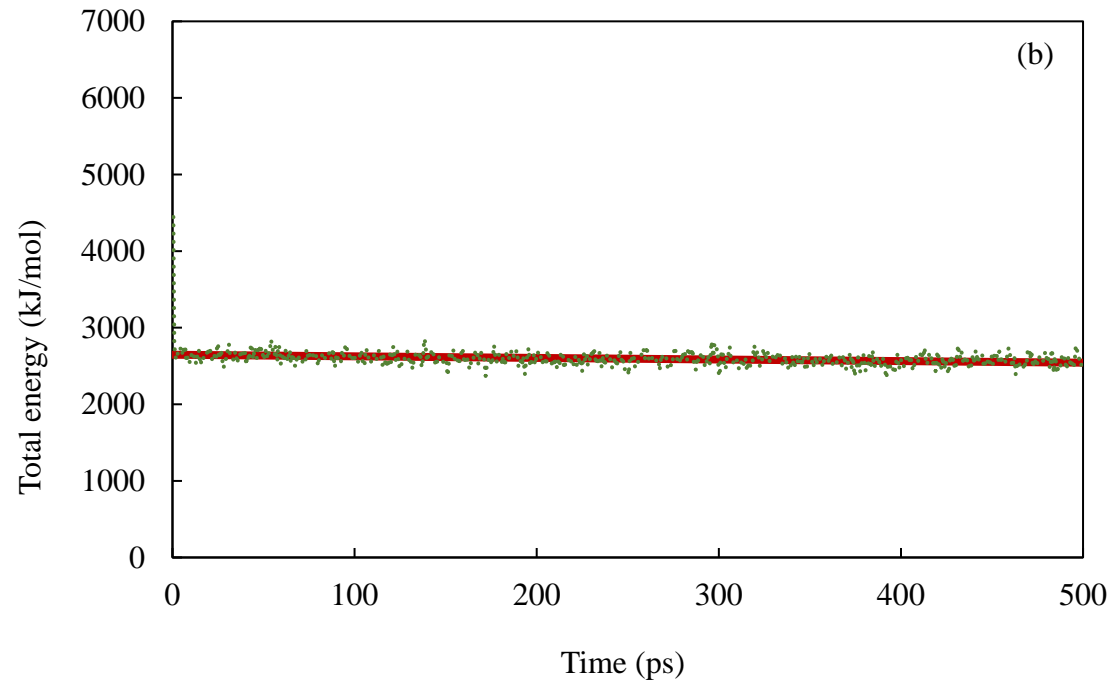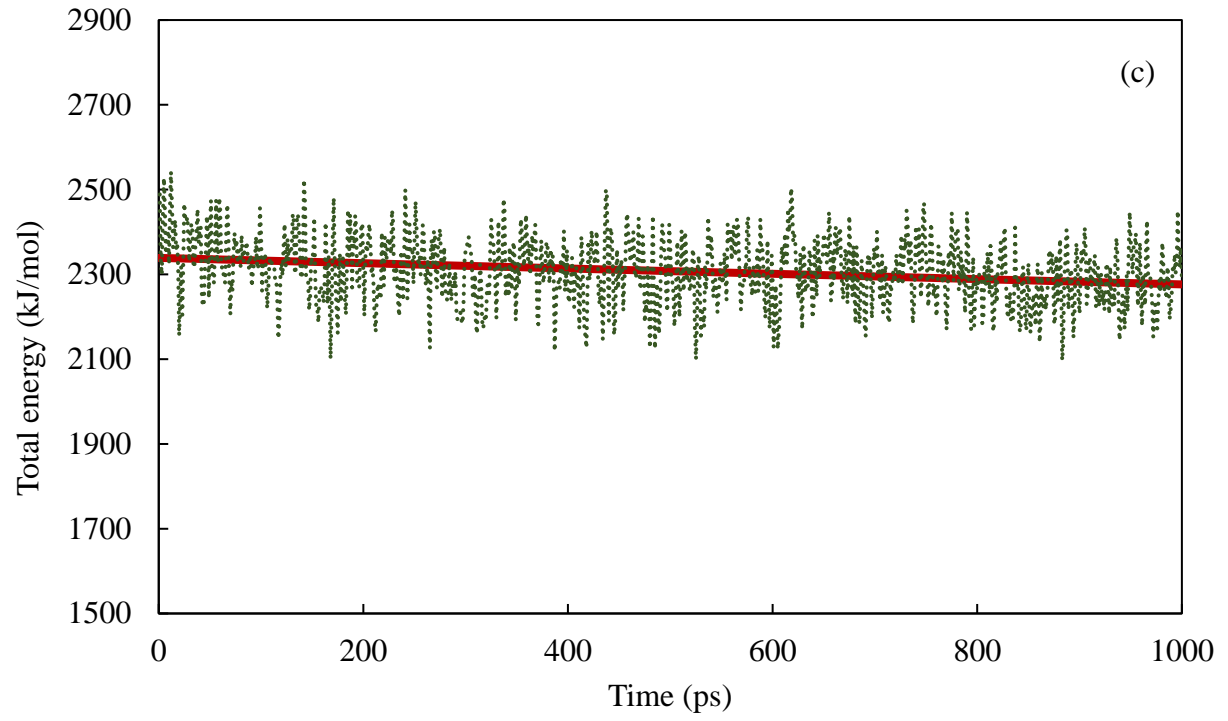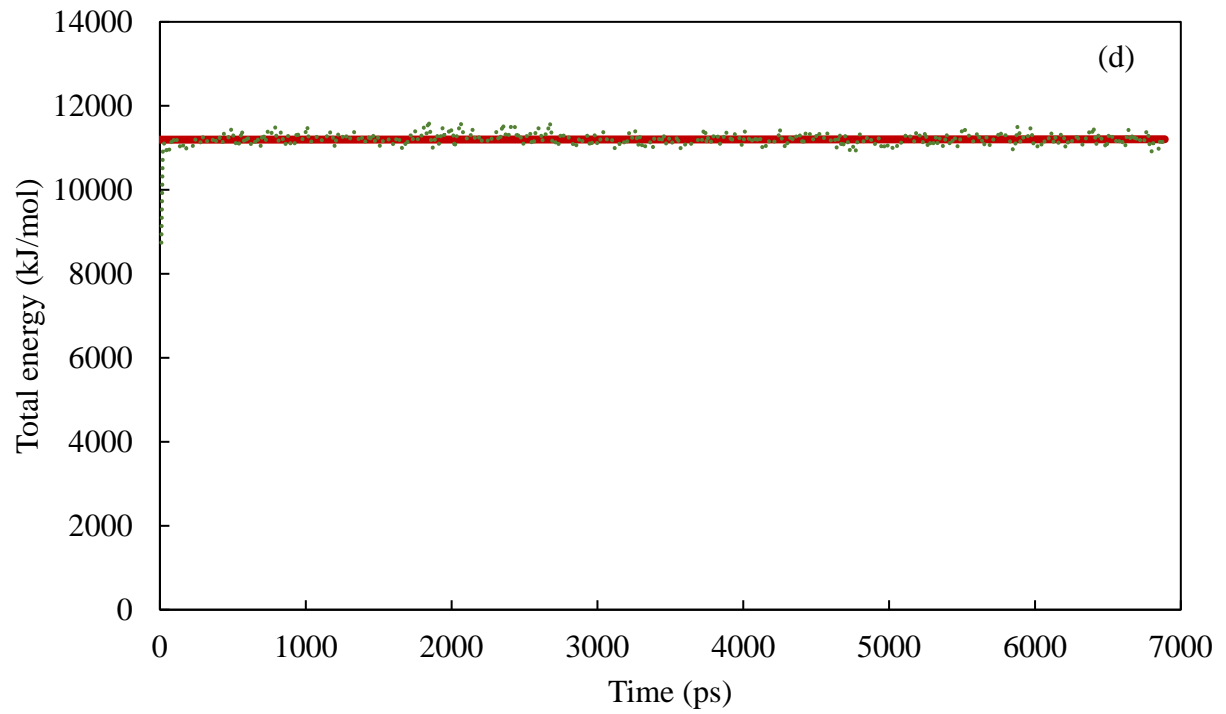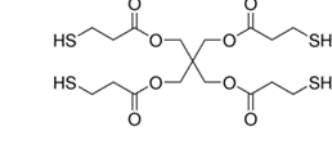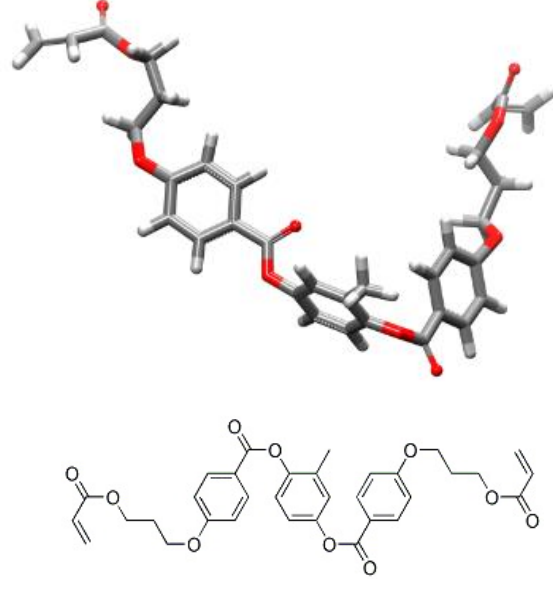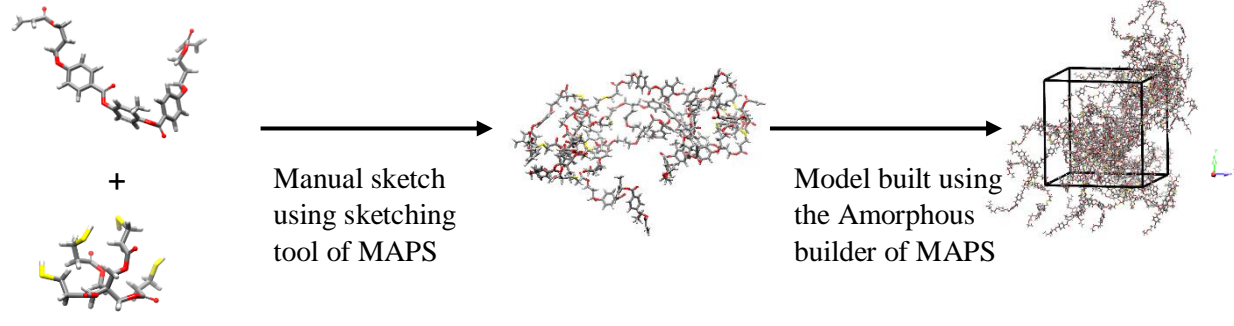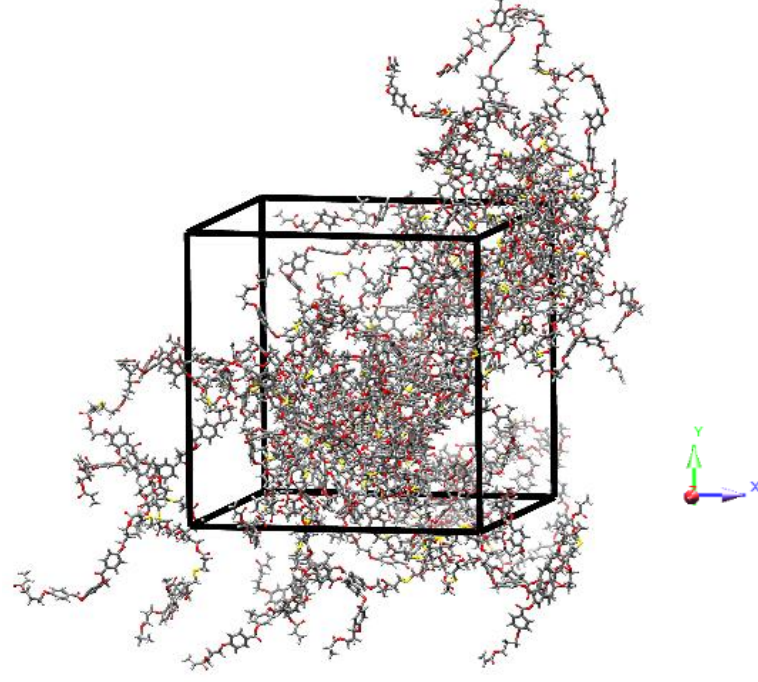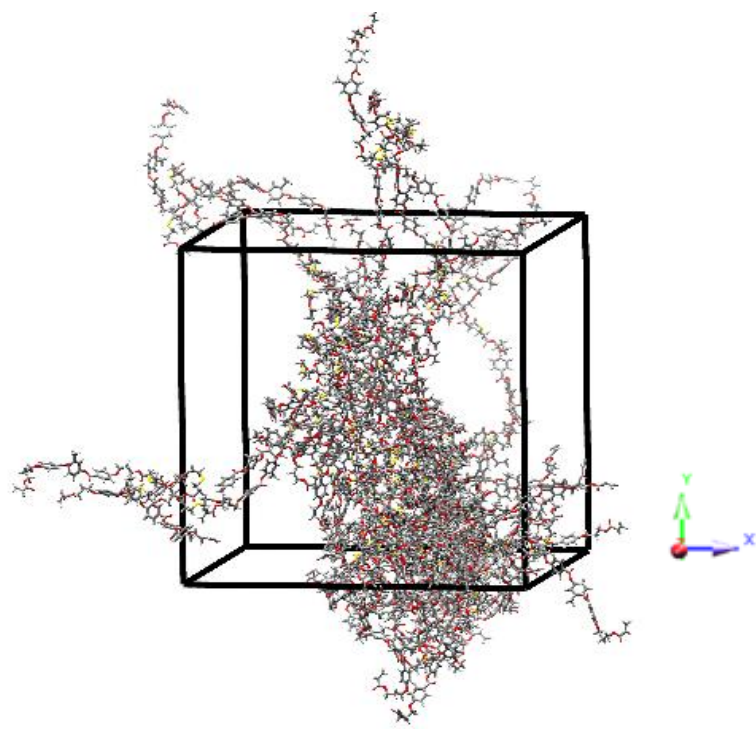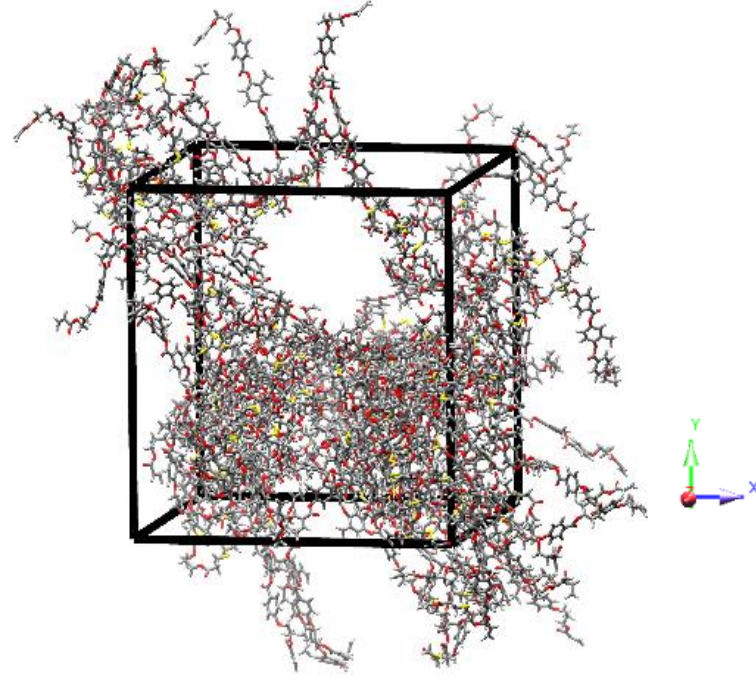
PLEASE CITE THIS ARTICLE AS DOI: 10.1063/5.0044197

AIP
Publishing

REFERENCES

1. T. Xie, Polymer **52,** 4985 (2011).
2. D. Ratna and J. Karger-Kocsis, Journal of Materials Science **43,** 254 (2008).
3. A. Lendlein and S. Kelch, Angewandte Chemie International Edition **41,** 2034 (2002).
4. P. Prathumrat, S. Tiptipakorn, and S. Rimdusit, Smart Materials and Structures **26,** 065025 (2017).
5. Y. Zhang, J. Liao, T. Wang, W. Sun, and Z. Tong, Advanced Functional Materials **28,** 1707245 (2018).
6. Y. Guo, Z. Lv, Y. Huo, L. Sun, S. Chen, Z. Liu, C. He, X. Bi, X. Fan, and Z. You, Journal of Materials Chemistry B **7,** 123 (2019).
7. J. Ban, L. Mu, J. Yang, S. Chen, and H. Zhuo, Journal of Materials Chemistry A **5,** 14514 (2017).
8. Y. Xie, Y. Meng, W. Wang, E. Zhang, J. Leng, and Q. Pei, Advanced Functional Materials **28,** 1802430 (2018).
9. S. Conti, M. Lenz, M. Pawelczyk, and M. Rumpf, in *Shape Optimization, Homogenization and Optimal Control* (Springer, 2018), p. 1.
10. X. Wu, Y. Han, Z. Zhou, X. Zhang, and C. Lu, ACS applied materials & interfaces **9,** 13657 (2017).
11. Q. Meng and J. Hu, Composites Part A: Applied Science and Manufacturing **40,** 1661 (2009).
12. C. Liu, H. Qin, and P. T. Mather, Journal of Materials Chemistry **17,** 1543 (2007).
13. H. Meng and G. Li, Polymer **54,** 2199 (2013).
14. B. Liu, Z. Tang, Z. Wang, L. Zhang, and B. Guo, Polymer **184,** 121914 (2019).
15. Z. Li, K. Li, H. He, Y. Zhou, and Z. He, Iranian Polymer Journal **28,** 371 (2019).
16. Y. J. Wang, U. S. Jeng, and S. H. Hsu, ACS Biomaterials Science & Engineering **4,** 1397 (2018).
17. X. Zhang, C. Zhu, B. Xu, L. Qin, J. Wei, and Y. Yu, ACS applied materials & interfaces **11,** 46212 (2019).
18. Z. Tang, J. Huang, B. Guo, L. Zhang, and F. Liu, Macromolecules **49,** 1781 (2016).
19. C. Wang, H. Wang, F. Zou, S. Chen, and Y. Wang, Polymers **11,** 1030 (2019).
20. F. Ji, J. B. Li, Y. X. Weng, and J. Ren, Materials Research Express **7,** 14 (2020).
21. P. Degennes, Comptes Rendus Hebdomadaires Des Seances De L Academie Des Sciences Serie B **281,** 101 (1975).
22. M. Warner and E. M. Terentjev, *Liquid crystal elastomers*, Vol. 120 (Oxford university press, 2007).
23. Y. Sagara and T. Kato, Nature chemistry **1,** 605 (2009).
24. H. Tong, S. Sengupta, and H. Tanaka, Nature communications **11,** 1 (2020).
25. T. J. White and D. J. Broer, Nature Materials **14,** 1087 (2015).
26. J. Küpfer and H. Finkelmann, Die Makromolekulare Chemie, Rapid Communications **12,** 717 (1991).
27. Y. Li, C. Pruitt, O. Rios, L. Wei, M. Rock, J. K. Keum, A. G. McDonald, and M. R. Kessler, Macromolecules **48,** 2864 (2015).
28. Z. Wen, M. K. McBride, X. Zhang, X. Han, A. M. Martinez, R. Shao, C. Zhu, R. Visvanathan, N. A. Clark, Y. Wang, K. Yang, and C. N. Bowman, Macromolecules **51,** 5812 (2018).
29. D. J. Davies, A. R. Vaccaro, S. M. Morris, N. Herzer, A. P. Schenning, and C. W. Bastiaansen, Advanced Functional Materials **23,** 2723 (2013).
30. N. Traugutt, R. Volpe, M. Bollinger, M. O. Saed, A. Torbati, K. Yu, N. Dadivanyan, and C. Yakacki, Soft Matter **13,** 7013 (2017).
31. T. H. Choi, S. M. Do, B. G. Jeon, S. T. Shin, and T. H. Yoon, Scientific Reports **9,** 10288 (2019).
32. M. Barnes and R. Verduzco, Soft Matter **15,** 870 (2019).
33. K. M. Lee, H. Koerner, R. A. Vaia, T. J. Bunning, and T. J. White, Soft Matter **7,** 4318 (2011).

[34] K. M. Lee, T. J. Bunning, and T. J. White, Advanced Materials **24,** 2839 (2012).

[35] E. H. Darzehkonani, in *Molecular dynamics simulation of planar extensional and shear rheology of dendritic and blended dendrimer-linear polymer melts*, 2015.

[36] K. Prasad, M. Nikzad, C. M. Doherty, and I. Sbarski, Polymer International **67,** 717 (2018).

[37] K. Vanommeslaeghe, E. Hatcher, C. Acharya, S. Kundu, S. Zhong, J. Shim, E. Darian, O. Guvench, P. Lopes, and I. Vorobyov, Journal of computational chemistry **31,** 671 (2010).

[38] H. Heinz, T. J. Lin, R. Kishore Mishra, and F. S. Emami, Langmuir **29,** 1754 (2013).

[39] G. Skačej and C. Zannoni, Soft Matter **7,** 9983 (2011).

[40] J. M. Ilnytskyi, M. Saphiannikova, D. Neher, and M. P. Allen, Soft Matter **8,** 11123 (2012).

[41] J. Diani and K. Gall, Smart materials and structures **16,** 1575 (2007).

[42] J. Moon, J. Choi, and M. Cho, Polymer **102,** 1 (2016).

[43] H. Yang, X. Zheng, Y. Sun, K. Yu, M. He, and Y. Guo, Computational Materials Science **139,** 48 (2017).

[44] X. J. Zhang, Q. S. Yang, X. Liu, J. J. Shang, and J. S. Leng, Smart Materials and Structures **29,** 015040 (2019).

[45] X. Wang, C. Tang, Q. Wang, X. Li, and J. Hao, Energies **10,** 1377 (2017).

[46] I. H. Sahputra, A. Alexiadis, and M. J. Adams, Molecular Simulation **44,** 774 (2018).

[47] M. O. Saed, A. H. Torbati, D. P. Nair, and C. M. Yakacki, JoVE (Journal of Visualized Experiments)**,** e53546 (2016).

[48] S. L. Mayo, B. D. Olafson, and W. A. Goddard, The Journal of Physical Chemistry **94,** 8897 (1990).

[49] H. Sun, Journal of Computational Chemistry **15,** 752 (1994).

[50] K. Prasad, M. Nikzad, C. M. Doherty, and I. Sbarski, Journal of Applied Polymer Science **136,** 48189 (2019).

[51] S. W. Bae and S. G. Cho, Journal of Molecular Modeling **22,** 147 (2016).

[52] D. Dubbeldam, K. S. Walton, T. J. H. Vlugt, and S. Calero, Advanced Theory and Simulations **2,** 1900135 (2019).

[53] J. Kuntail, S. Pal, and I. Sinha, Journal of Molecular Liquids **318,** 114037 (2020).

[54] M. G. Martin and A. P. Thompson, Fluid phase equilibria **217,** 105 (2004).

[55] P. G. Boyd, S. M. Moosavi, M. Witman, and B. Smit, The journal of physical chemistry letters **8,** 357 (2017).

[56] K. Prasad, M. Nikzad, and I. Sbarski, Journal of Applied Polymer Science **137,** 49220 (2020).

[57] Q. Huang, X. Yang, and X. He, Discrete & Continuous Dynamical Systems-B **23,** 2177 (2018).

[58] P. K. Mukherjee and T. B. Mukherjee, Physical Review B **52,** 9964 (1995).

[59] B. Roie, J. Leys, K. Denolf, C. Glorieux, G. Pitsi, and J. Thoen, Physical review. E, Statistical, nonlinear, and soft matter physics **72,** 041702 (2005).

[60] M. Zhou, X. Xiong, D. Drummer, and B. Jiang, Polymers **11,** 557 (2019).

[61] M. O. Saed, R. H. Volpe, N. A. Traugutt, R. Visvanathan, N. A. Clark, and C. M. Yakacki, Soft Matter **13,** 7537 (2017).

[62] C. Li, E. Coons, and A. Strachan, Acta Mechanica **225,** 1187 (2014).

[63] G. Odegard, T. Clancy, and T. Gates, in *Prediction of mechanical properties of polymers with various force fields*, 2005, p. 1850.

[64] W. K. Goertzen and M. Kessler, Composites Part B: Engineering **38,** 1 (2007).

[65] H. Sun, The Journal of Physical Chemistry B **102,** 7338 (1998).

[66] T. C. Lim, Zeitschrift für Naturforschung A **64,** 200 (2009).

[67] G. Sutmann; *Vol. 10* (John von Neumann Institute for Computing, Jülich, 2002), p. 211.

[68] D. L. Cheung, S. J. Clark, and M. R. Wilson, Physical Review E **65,** 051709 (2002).

[69] P. Zhang and G. Li, Journal of Polymer Science Part B: Polymer Physics **51,** 966 (2013).

[70] A. Martínez-Gómez, J. P. Fernández-Blázquez, A. Bello, and E. Pérez, Macromolecules **49,** 5306 (2016).

[71] B. C. Abberton, W. K. Liu, and S. Keten, Journal of the Mechanics and Physics of Solids **61,** 2625 (2013).

1

2

3

4

5

         (a)   (b)

6   FIG. 1. Chemical structures used in MD simulations of (a) RM257 monomer (C = grey, H = light grey, O = red), (b)

7   PETMP crosslinker (C = grey, O = red, H = light grey, S = yellow).

8

9

10

11

12

13

14

15

16

17

18

1

2

3

4

5   +

6

7

8

9

10

11

12

13

14

15

16   (a)

17

18

19

20

21

22   (c)

Manual sketch
using sketching
tool of MAPS

Model built using
the Amorphous
builder of MAPS

(b)

FIG. 2. Sketch of LCE and crosslinking agent for building the main-chain elastomer model. The main-chain LCEs
were subjected to three force fields; (a) Dreiding, (b) PCFF and (c) SciPCFF.

23

24

25

26

17

1
2
3
4
5
6
7
8
9
10
11
12
13
14
15

FIG. 3. Steady-state density of liquid crystalline monomers under different force fields (a) Dreiding, (b) PCFF and (c) SciPCFF.

16
17
18
19
20
21
22
23

1

2

3

4

5

6

7

8

9

10

11

12

13

14

15

16

17

18

19

20

21

22

23

24   FIG. 4. Fractional free volume versus temperature plot of LCE of three force fields (a) Dreiding, (b) PCFF and (c)

25   SciPCFF.

26

1

FIG. 5. Experimental results of storage modulus and tan delta of modelled LCE, with T_{NI} at 87ºC (from tan delta).

3

4

FIG. 6. Storage modulus at various temperature of the modelled LCE under different force fields compared with experimental result.

7

FIG. 7. Relative storage modulus at various temperature of LCE under different force fields compared with experimental results.

FIG. 8. A comparison of simulated tan delta of LCE for different force fields with experimental results.

1

2

3

4

5

6

7

8

9

10

11

12

13   FIG. 9. Scheme of a four-step shape memory process with tensile mode.

14

1

2

1

2

3

FIG. 10. Pressure of the model during the various steps of shape memory process; (a) deforming step, (b) cooling step,

(c) unloading step and (d) reheating step.

1

2

1

2

3

4   FIG. 11. Total energy of various step of shape memory process; (a) deforming step, (b) cooling step, (c) unloading

5   step and (d) reheating step.

Manual sketch
using sketching
tool of MAPS

Model built using
the Amorphous
builder of MAPS

+

(a)

(b)

(c)

(106ºC, 36%)

(a)

(73ºC, 34%)

(b)

(77ºC, 31%)

(c)

Δx

1. Loading step
NPT, 400K 1atm, 5 ns

Original shape

Stretched shape

2. Cooling step
NVT, 298K 1atm, 500 ps

Thermomechanical shape memory
process

Cooling shape

4. Reheating step
NPT, 450K 1atm, 10 ns

Original shape

Temporary shape

3. Unloading step
NPT, 298K 1atm, 1 ns

(b)

(a)

Author/s:
Prathumrat, P; Sbarski, I; Hajizadeh, E; Nikzad, M

Title:
A comparative study of force fields for predicting shape memory properties of liquid crystalline elastomers using molecular dynamic simulations